Supplementary material for Optical properties of the perfectly compensated semimetal WTe_2

C. C. Homes,[1,*] M. N. Ali,[2] and R. J. Cava[2]

[1] *Condensed Matter Physics and Materials Science Department, Brookhaven National Laboratory, Upton, New York 11973, USA*

[2] *Department of Chemistry, Princeton University, Princeton, New Jersey 08544, USA*

(Dated: September 9, 2015)

ELECTRONIC STRUCTURE CALCULATIONS

Tungsten ditelluride, WTe_2, crystallizes in the orthorhombic $Pmn2_1$ space group [1], where the tungsten atoms form chains along the a axis and lie between sheets of tellurium atoms, forming the a-b planes; the unit cell is reproduced from the main text in Fig. S1 for convenience. The electronic structure of WTe_2 was calculated using both the local spin density approximation (LSDA) as well as the generalized gradient approximation (GGA) using the full-potential linearized augmented plane-wave (FP-LAPW) method [2] with local-orbital extensions [3] in the WIEN2k implementation [4]. The system was assumed to be non-magnetic. An examination of different Monkhorst-Pack k-point meshes indicated that a $9 \times 5 \times 2$ mesh and $R_{mt}k_{max} = 7.75$ was sufficient for good energy convergence. The geometry of the unit cell was refined through an iterative process whereby the volume was optimized with respect to the total energy while the c/a ratio remained fixed. The atomic fractional coordinates were then relaxed with respect to the total force, typically resulting in residual forces of less than 0.2 mRy/a.u. For both of these procedures spin-orbit coupling is ignored. This approach was repeated until no further improvement was obtained. A comparison of the experimental and calculated (relaxed) unit cell parameters are shown in Table. I.

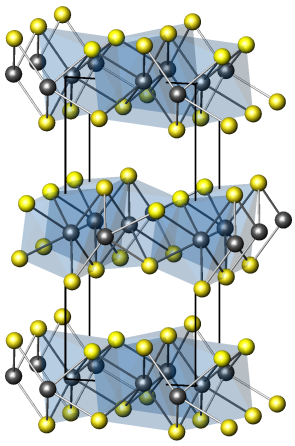

Figure S1. (Color online) The unit cell is shown for the b-c face projected along the a axis. The tungsten atoms are surrounded by tellurium octahedra that are distorted due to the zig-zag nature of the tungsten chains.

The electronic band structure has been calculated with LSDA and spin-orbit coupling for several different paths between high-symmetry points in the orthorhombic unit cell, shown in Fig. S2. This calculation accurately reproduces the work of Ali *et al.* [5], as well as an earlier work [6]. The relatively small number of bands crossing the Fermi level (ϵ_F) illustrates the semimetallic character of WTe_2. In particular, there is an electron-like band and a hole-like band crossing Fermi surface along the $\Gamma - X$ direction. Figure S2 also reveals that there are several other points in the Brillouin zone at which hole and electron bands just manage to cross the Fermi surface; however, the electronic structure is quite sensitive to the unit cell geometry, and that even a small increase (or decrease) in the Fermi level might move these bands above or below ϵ_F. While the paths along the high-symmetry directions are useful, the contributions of the hole and electron bands to the transport is best understood

Table I. The experimental and theoretical lattice constants and atomic fractional coordinates for the relaxed structure of WTe_2 in the orthorhombic $Pmn2_1$ space group.

	Experiment[a]		Theory (LSDA)		Theory (GGA)	
a(Å)	3.5306		3.4657		3.5423	
b(Å)	6.3443		6.2274		6.3653	
c(Å)	14.2123		13.9509		14.2595	
W1 ($\frac{1}{2}xy$)	0.39890	0.50030	0.39866	0.50076	0.39859	0.50039
W2 ($0xy$)	0.04310	0.48490	0.04368	0.48491	0.04393	0.48502
Te1 ($\frac{1}{2}xy$)	0.79410	0.59540	0.79507	0.59548	0.79470	0.59428
Te1 ($0xy$)	0.30040	0.63990	0.29920	0.64169	0.30052	0.63948
Te1 ($0xy$)	0.85620	0.84510	0.85526	0.84396	0.85649	0.84588
Te1 ($\frac{1}{2}xy$)	0.35180	0.89020	0.35271	0.89030	0.35225	0.89129

[a] Ref. 1.

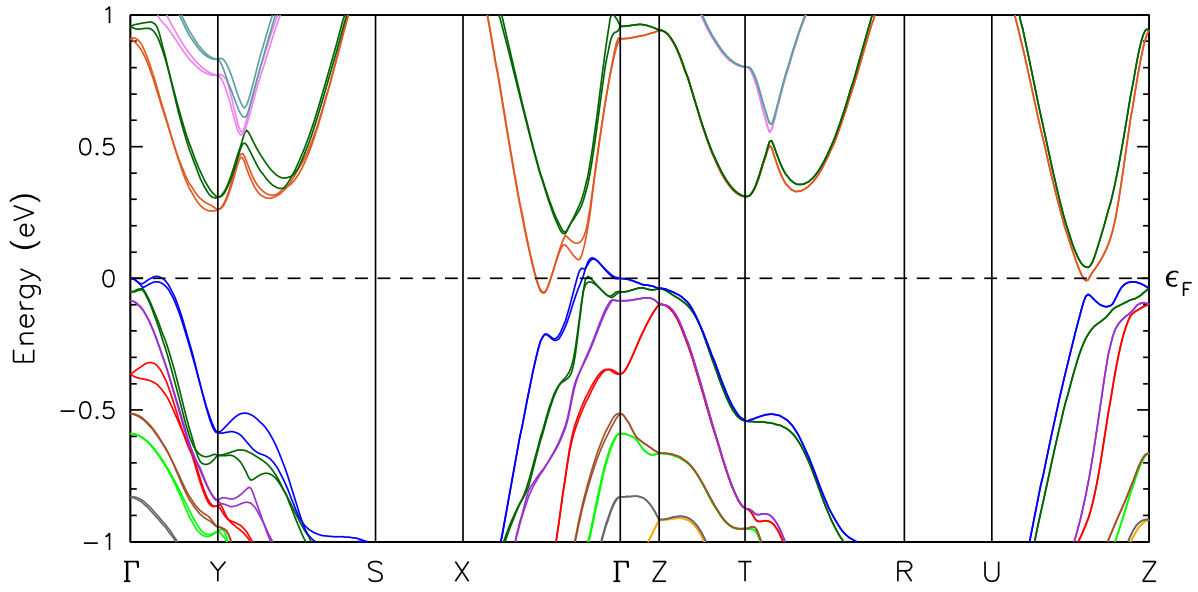

Figure S2. (Color online) The calculated LSDA electronic band structure of WTe_2 including the effects of spin-orbit coupling shown for several different paths between high-symmetry points for an orthorhombic Brillouin zone (generated using 500 k points).

from the nature of the Fermi surface.

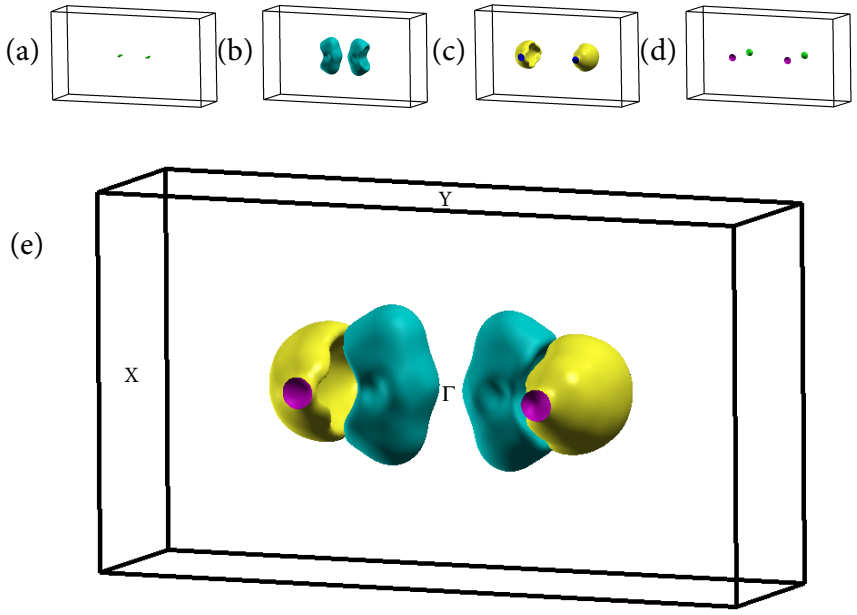

Figure S3. (Color online) The (a) small and (b) large hole LSDA Fermi surfaces. (c) Large and (d) small electron Fermi surfaces. (e) The merged Fermi surface of the electron (yellow) and hole (blue) pockets in the orthorhombic Brillouin zone along the $\Gamma - X$ direction.

FERMI SURFACE

The Fermi surface has been calculated using LSDA and a dense k-point mesh (10 000 k points, resulting in a $41 \times 23 \times 10$ mesh)[7]. The resulting Fermi surface is shown in Fig. S3 and consists of a total of four pockets; two hole pockets, one small and one large, shown in Figs. S3(a) and (b), respectively, and two electron pockets, one large and one small, shown in Figs. S3(c) and (d), respectively. The merged Fermi surface shown in Fig. S3(e) consists of the electron (yellow) and hole (blue) pockets slightly displaced from the origin of the Brillouin zone along the $\Gamma - \mathrm{X}$ direction, in agreement with a previous calculation [5] and several experimental observations [8, 9].

DIELECTRIC TENSOR

In the main text the real part of the optical conductivity has been calculated [10] from the the imaginary part of the dielectric function, $\sigma_{x,x} = 2\pi\omega\,\Im\,\epsilon_{x,x}/Z_0$, using a fine k point mesh (10 000 k points, yielding a $41 \times 23 \times 10$ mesh); $Z_0 \approx 377\,\Omega$ is the impedance of free space, resulting the units for the conductivity of $\Omega^{-1}\mathrm{cm}^{-1}$.

In this case, the free-carrier contribution is not calculated, so that the imaginary part of the dielectric function is the sum of the contributions to the dielectric tensor over all the allowed interband transitions. There are a total of 617 energy bands, with the last occupied band occurring at 276. Only direct ($\mathbf{q} = 0$) transitions are considered from occupied to unoccupied states; this being the case, the bands near the Fermi surface will be of particular importance as they will make the most significant contributions to the imaginary part of the dielectric function and thus the optical conductivity. The energy bands within 1 eV of the Fermi level along the $\Gamma - \mathrm{X}$ direction have been labeled in Fig S4. Note that in the main text both $\sigma_{x,x}$ and $\sigma_{y,y}$ have been calculated; however, whereas $\sigma_{x,x}$ displays prominent structures at 650 cm^{-1} (80 meV) and 1300 cm^{-1} (160 meV), the first prominent feature in $\sigma_{y,y}$ only occurs at about 1300 cm^{-1}, therefore this calculation will focus on the result for imaginary part of $\epsilon_{x,x}$ [11]. Transitions between all energy bands have calculated; however, we will only consider contributions to $\Im\,\epsilon_{x,x} \gtrsim 0.5$. These transitions are shown in Fig. S5. For bands 235 and 236, there are only weak contributions from transitions to bands 241 and 242 that only occur at energies above about 3400 cm^{-1} (420 meV); however, for bands 237 and 238, we see contributions from an increasing number of bands ($239 \rightarrow 244$) with a much lower onset of about 400 cm^{-1} (50 meV) with noticeable peaks at about 700 (87 meV) and 2500 cm^{-1} (310 meV). The contribution from band 239 is particulary interesting as there is an unusually low-energy transition at about 150 cm^{-1} (19 meV) with another prominent absorption at 1400 cm^{-1} (174 meV); for band 240 the strongest absorption is at about 800 cm^{-1} (99 meV). For bands 241 and 242, the remaining contributions are fairly small. Thus, the two strongest contributions are from the transitions $239 \rightarrow 242$ and $240 \rightarrow 241$, which are the energy bands related to the electron and hole pockets that form the Fermi surface so we may conclude that the low-energy interband transitions originate from these energy bands.

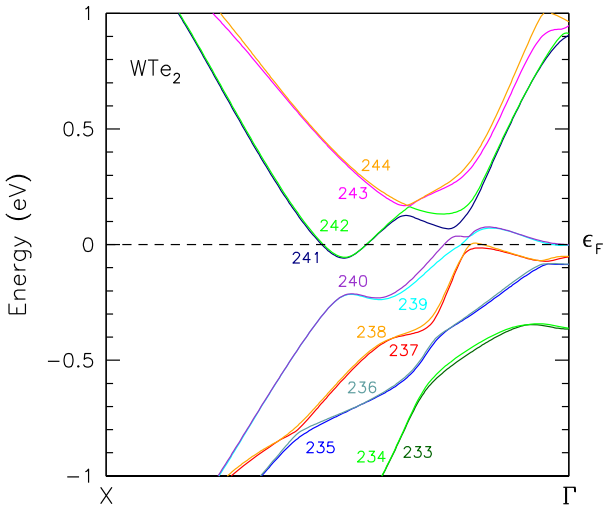

Figure S4. (Color online) The indexed LSDA energy bands near the Fermi level along the $\Gamma - \mathrm{X}$ direction in the orthorhombic Brillouin zone.

The sum of all of the contributions to the imaginary part of the complex dielectric function $\Im\,\epsilon_{x,x}$ is shown in Fig. S6, with the calculated real part of the optical conductivity shown in the inset [note this is same quantity that is shown in Fig. 4(c)]. The peak at about 150 cm^{-1}, while prominent in the imaginary part of $\epsilon_{x,x}$, is diminished in the optical conductivity due to the effects of frequency scaling.

* homes@bnl.gov

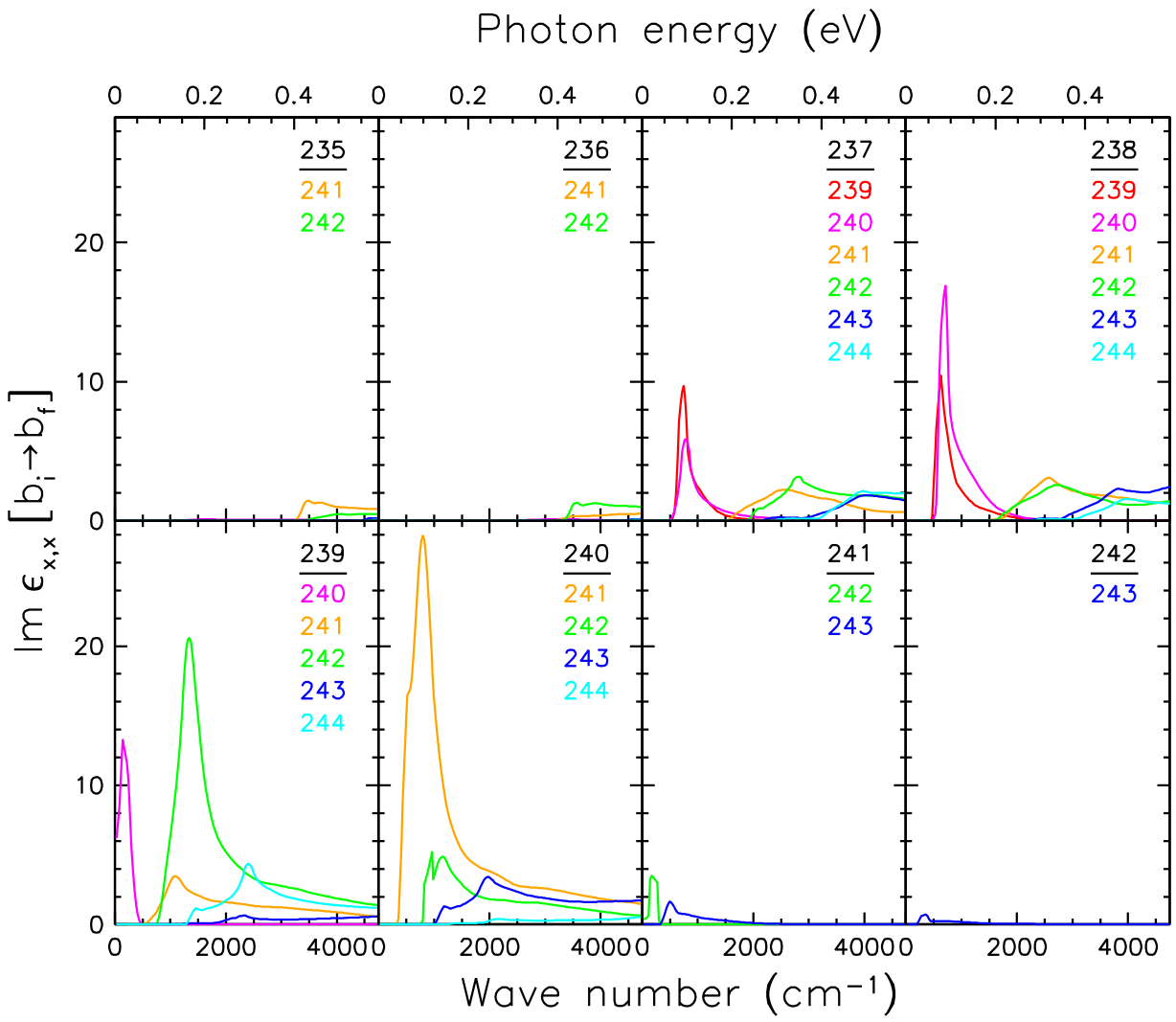

Figure S5. (Color online) The LSDA contributions to the imaginary part of the dielectric function $\Im\,\epsilon_{x,x}$ for the various transitions between occupied (b_i) to unoccupied (b_f) bands, beginning at 235 and ending at 242. In each panel, the initial band is above the horizontal line, while the final band (or bands) is listed below the line; note that the choice of bands was determined from the criteria at the contribution should be larger than $\simeq 0.5$.

[1] A. Mar, S. Jobic, and J. A. Ibers, "Metal-metal vs tellurium-tellurium bonding in WTe_2 and its ternary variants $TaIrTe_2$ and $NbIrTe_4$," J. Am. Chem. Soc. **114**, 8963–8971 (1992).

[2] D. J. Singh, *Planewaves, Pseudopotentials and the LAPW method* (Kluwer Adademic, Boston, 1994).

[3] David Singh, "Ground-state properties of lanthanum: Treatment of extended-core states," Phys. Rev. B **43**, 6388–6392 (1991).

[4] P. Blaha, K. Schwarz, G. K. H. Madsen, D. Kvasnicka and J. Luitz, WIEN2k, *An augmented plane wave plus local orbitals program for calculating crystal properties* (Techn. Universität Wien, Austria, 2001).

[5] Mazhar N. Ali, Jun Xiong, Steven Flynn, Jing Tao, Quinn D. Gibson, Leslie M. Schoop, Tian Liang, Neel Haldolaarachchige, Max Hirschberger, N. P. Ong, and R. J. Cava, "Large, non-saturating magnetoresistance in WTe_2," Nature (London) **514**, 205208 (2014).

[6] J. Augustin, V. Eyert, Th. Böker, W. Frentrup, H. Dwelk, C. Janowitz, and R. Manzke, "Electronic band structure of the layered compound Td – WTe_2," Phys. Rev. B **62**, 10812–10823 (2000).

[7] Anton Kokalj, "Computer graphics and graphical user interfaces as tools in simulations of matter at the atomic scale," Comp. Mat. Sci. **28**, 155–168 (2003).

[8] I. Pletikosić, Mazhar N. Ali, A. V. Fedorov, R. J. Cava, and T. Valla, "Electronic Structure Basis for the Extraordinary Magnetoresistance in WTe_2," Phys. Rev. Lett. **113**, 216601 (2014).

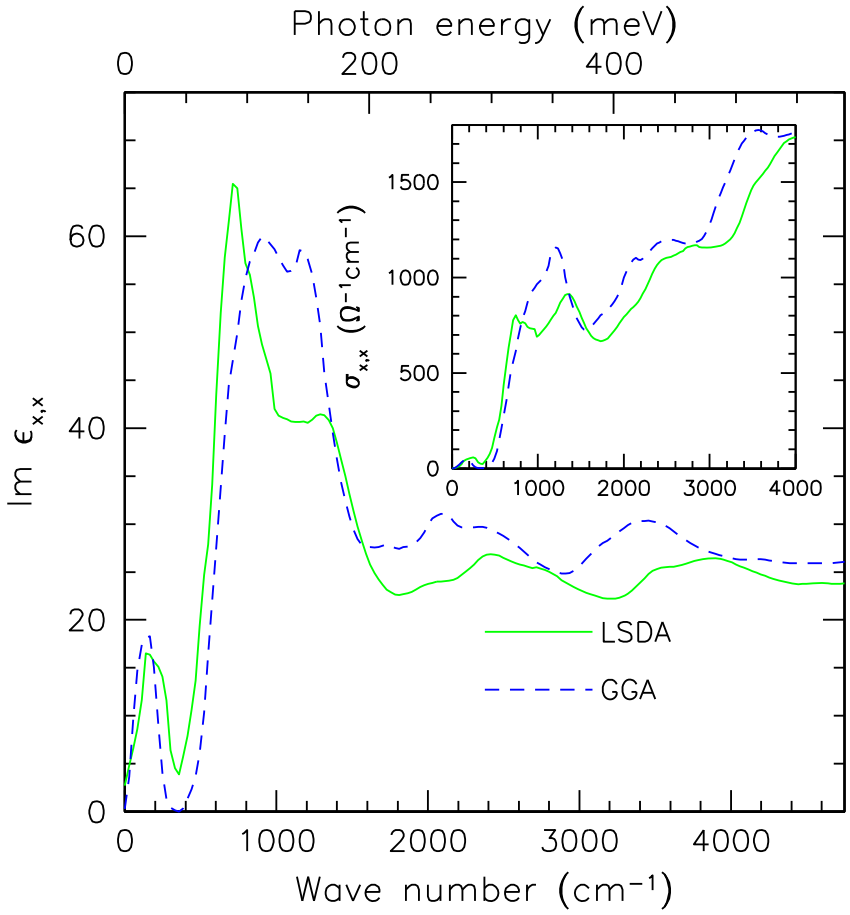

Figure S6. (Color online) The imaginary part of the dielectric function $\epsilon_{x,x}$ from a summation of all of the individual interband contributions, determined using LSDA (solid line) and GGA (dashed line) with spin-orbit coupling. Inset: The real part of the optical conductivity $\sigma_{x,x}$ calculated from the imaginary part of complex dielectric function $\epsilon_{x,x}$ using LSDA (solid line) and GGA (dashed line).

[9] J. Jiang, F. Tang, X. C. Pan, H. M. Liu, X. H. Niu, Y. X. Wang, D. F. Xu, H. F. Yang, B. P. Xie, F. Q. Song, X. G. Wan, and D. L. Feng, "Signature of strong spin-orbital coupling in the large non-saturating magnetoresistance material WTe_2," arXiv:1503.01422 [cond-mat].

[10] Claudia Ambrosch-Draxl and Jorge O. Sofo, "Linear optical properties of solids within the full-potential linearized augmented planewave method," Comp. Phys. Commun. **175**, 1–14 (2006).

[11] It is convenient to recall that $1\,\mathrm{eV} = 8065.5\,\mathrm{cm}^{-1}$.